

Low-density phases of ^3He monolayers adsorbed on graphite

Michele Ruggieri,¹ Ettore Vitali,² Davide Emilio Galli,³ Massimo Boninsegni,⁴ and Saverio Moroni^{5,1}

¹*SISSA Scuola Internazionale Superiore Studi Avanzati, Via Bonomea 265, I-34136 Trieste, Italy*

²*Department of Physics, The College of William and Mary, Williamsburg, Virginia 23187*

³*Dipartimento di Fisica, Università degli Studi di Milano, via Celoria 16, 20133 Milano, Italy*

⁴*Department of Physics, University of Alberta, Edmonton, Alberta, Canada, T6G 2E1*

⁵*CNR-IOM DEMOCRITOS Simulation Center, Via Bonomea 265, I-34136 Trieste, Italy*

(Received 12 December 2015; revised manuscript received 10 February 2016; published 2 March 2016)

Quantum Monte Carlo simulations at zero temperature of a ^3He monolayer adsorbed on graphite, either clean or preplated with ^4He , unexpectedly point to a gas-liquid phase transition at a very low areal density of the order of 0.01 \AA^{-2} . This result stems from an essentially unbiased calculation of the ground-state energy for an infinite, defect-free substrate, which interacts with He atoms via a realistic potential, whereas the interaction between two He atoms includes two- and three-body terms. The sensitivity of the gas-liquid coexistence region on the model Hamiltonian employed is discussed.

DOI: [10.1103/PhysRevB.93.104102](https://doi.org/10.1103/PhysRevB.93.104102)

I. INTRODUCTION

Thin films of either isotope of He adsorbed on substrates have been widely studied experimentally as close realizations of ideal, strictly two-dimensional (2D) quantum systems with a coupling strength tunable by varying the coverage. For example, specific heat and magnetization measurements on the first and second adlayers of ^3He on graphite give very similar results [1–3], structural differences between successive monolayers notwithstanding. Thus these layers are deemed to provide a close realization of the 2D model, allowing one to obtain experimentally estimates of such fundamental properties of 2D Fermi liquid as the effective mass and spin susceptibility. Likewise, the superfluid transition of a ^4He liquid adlayer has been predicted [4] and observed [5–8] to adhere rather closely to the 2D (Kosterlitz-Thouless) paradigm [9].

Figure 1 shows the zero-temperature equations of state (energy per particle E versus density ρ) of 2D ^4He , ^3He , and a fictitious bosonic version of spin-zero ^3He , computed in this work as described below. The results are in agreement with those of previous, comparable calculations [10–15], with only minimal differences arising from the use of slightly different interatomic potentials. As one can see, ^4He features a self-bound liquid phase of equilibrium density $\rho_0 = 0.044 \text{ \AA}^{-2}$, below which the system forms puddles; on the other hand, ^3He remains in a homogeneous fluid phase from the crystallization density all the way down to the ideal gas limit. The difference between ^3He and ^4He arises because of the higher kinetic energy of ^3He , which is due in part to its lighter mass, and in part to Fermi statistics—the latter being at the root of the qualitatively different shape of the $E(\rho)$ curve for ^3He , compared to that for ^4He and bosonic spin-zero ^3He , also a self-bound liquid.

Although no liquid phase of ^3He exists in purely 2D, there are reasons to expect that it may in quasi-2D, i.e., in a thin film adsorbed on a suitable substrate. This is because adatoms experience two distinct effects which favor the formation of a liquid phase of ^3He (and enhance the stability of that of ^4He), compared to the strictly 2D case. The first is

quantum delocalization in the direction perpendicular to the substrate, which acts to soften the hard-core repulsion of the helium interatomic potential at short distances; the second is substrate corrugation, which effectively increases the mass of the Helium atoms.

For example, on weakly attractive substrates such as those of alkali metals, where delocalization is significant and whose corrugation can be regarded as negligible, on account of the relatively large equilibrium distance of the atoms from the surface, ^3He has been predicted [16] to undergo a phase transition between a gas and a thermodynamically stable (albeit not self-bound) liquid, signalled by a local minimum in the equation of state $E(\rho)$.

The stability of the liquid phase weakens for increasingly attractive substrates, suggesting that ^3He may not condense into a stable liquid on a substrate as strong as graphite. On the other hand, as adatoms move closer to the surface, the enhancement of their effective mass arising from substrate corrugation may again underlie a thermodynamically stable liquid phase. More generally, the existence of a gas-liquid transition of a quasi-2D adsorbed ^3He film hinges on the interplay of a number of subtle, substrate-dependent effects.

Although the phase diagram of helium adsorbed on graphite has been extensively investigated experimentally, there is no general consensus about the existence of one or more fluid phases, even in the first ^3He adlayer. The prevailing opinion has been that ^3He should form a 2D gas at low coverage, directly crystallizing into a registered solid as coverage is increased; however, there exist conflicting theoretical predictions [11,12,17,18] and the lack of data at sufficiently low temperatures and coverage to provide a definitive experimental answer [19]. The issue has received renewed consideration after a recent measurement of the specific heat, whose linear dependence on the density at very low coverages has been interpreted in terms of puddles of self-bound liquid. Interestingly, similar results were reported for the first, second and third adlayers of ^3He on graphite [20].

In this work, we use quantum Monte Carlo simulations to calculate with high accuracy the $T = 0$ low-density equation of state (EOS) of ^3He on graphite (G), and on graphite

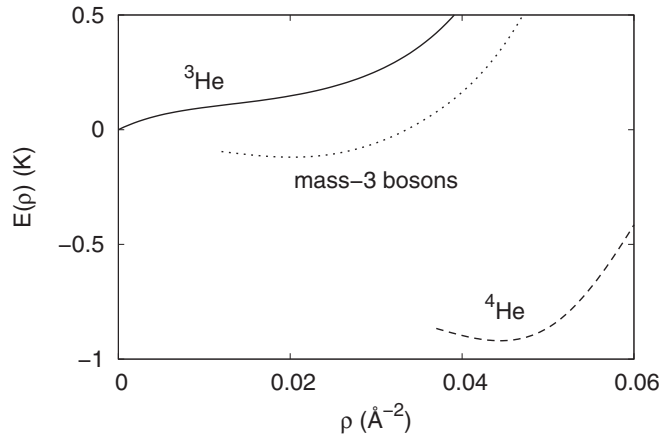


FIG. 1. Ground-state energy per atom $E(\rho)$ of 2D ${}^3\text{He}$ (solid line), ${}^4\text{He}$ (dashed line), and fictitious mass-3 bosonic Helium (dotted line). The global minima for ${}^4\text{He}$ and mass-3 bosons locate the equilibrium densities of the self-bound liquid phases, respectively 0.044 and 0.020 \AA^{-2} . For ${}^3\text{He}$, there is neither self-bound liquid nor gas-liquid phase transition.

preplated with a solid monolayer of ${}^4\text{He}$ (G4He). In both cases, the compressibility becomes negative in a small density region, implying a pressure-induced phase transition between a finite-density gas and a liquid.

This result falls short of providing a direct, unambiguous quantitative confirmation of the findings of Ref. [20], which is to be expected given the limitations of the (still relatively simplified) theoretical model utilized here. Nevertheless, it clearly lends support to the idea that a stable liquid phase may exist, one which in the case of G is crucially underlain by the substrate corrugation. The remainder of this article is organized as follows: in Sec. II, we describe the mathematical model and the computational methodology utilized in this work; Secs. III and IV are devoted to a thorough illustration of our results, and in particular, in Sec. IV, we offer specific, quantitative details, for the purpose of facilitating the task of others who may wish to reproduce our results. We outline our conclusions and prospects for further studies in Sec. V.

II. MODELS AND METHOD

We consider a system of N ${}^3\text{He}$ atoms in the presence of a planar substrate, enclosed in a cell of sides L_x , L_y , and L_z with periodic boundary conditions. The quantum-mechanical many-body Hamiltonian is the following:

$$H = -\lambda \sum_{i=1}^N \nabla_i^2 + V(R) + \sum_{i=1}^N U(\mathbf{r}_i), \quad (1)$$

where $\lambda = 8.0417 \text{ K \AA}^{-2}$, $R = \{\mathbf{r}_1, \dots, \mathbf{r}_N\}$ are the coordinates of the ${}^3\text{He}$ atoms, $V(R)$ is the He-He interaction, and $U(\mathbf{r})$ is the He-substrate interaction. The areal density of the system is defined as $\rho = N/(L_x L_y)$, with the z axis perpendicular to the substrate. As we aim to model the system as realistically as possible, in $V(R)$, we include the highly accurate, first-principles SAPT2 pair potential [21] and the Axilrod-Teller-Muto three-body potential [22,23], which at low density is by

far the most important term beyond pair-wise interactions [24]. Concerning the He-substrate interaction $U(\mathbf{r})$, for ${}^3\text{He}$ directly adsorbed on G we use the anisotropic potential of Carlos and Cole [25] (CC), which accounts for substrate corrugation and has been adopted in most computational studies of ${}^4\text{He}$ adsorbed on graphite [26–29]. For ${}^3\text{He}$ adsorbed on G4He instead, we derive an effective potential which is significantly weaker than for G and only depends on the z component of \mathbf{r} . Since the procedure is somewhat elaborate, we defer its discussion to Sec. IV to avoid diverting from the main results of this work.

The ground-state energy of the model Hamiltonian (1) is calculated by means of fixed-node diffusion Monte Carlo (FNDMC) [30–32], a widely used quantum Monte Carlo technique which gives very accurate energy upper bounds by projecting the lowest-energy fermion eigenstate of the Hamiltonian with the same nodes as a trial wave function Ψ . Specifically, FNDMC simulates the imaginary-time evolution of the system in configuration space through a branching random walk of a large (ideally infinite) number of walkers, subjected to the constraint that the nodes of Ψ never be crossed. Beside (i) the finite size of the system, FNDMC is subject to errors from (ii) the time discretization of the random walk, (iii) the finite number of walkers, and (iv) the fixed-node constraint. The errors due to (i)–(iii) can be estimated varying the number of particles, the time step, and the number of walkers, and eliminated by extrapolation whenever deemed non-negligible. The only uncontrolled error, namely the fixed-node approximation, depends on the nodal structure of Ψ .

The trial many-body wave functions used in this work have the Jastrow-Slater form $\Psi = \exp(-U)D_\uparrow D_\downarrow$. The Jastrow factor $U = U_1 + U_2 + U_3$ contains standard two- and three-body correlations between Helium atoms [33], as well as one-body Helium-substrate correlations:

$$\begin{aligned} U_1 &= \sum_i f(z_i) + \sum_{ij} g(|\mathbf{r}_i - \mathbf{t}_j|), \\ U_2 &= \sum_{i<j} u(r_{ij}), \\ U_3 &= \sum_{j \neq i} \xi(r_{ij})(\mathbf{r}_i - \mathbf{r}_j) \cdot \sum_{l \neq i} \xi(r_{il})(\mathbf{r}_i - \mathbf{r}_l). \end{aligned} \quad (2)$$

The second term in U_1 is a radial correlation between each helium atom and an array of sites placed at positions \mathbf{t}_j , shifted by an amount d above each carbon atom of the graphite surface. It is used only for the corrugated substrate.

In the Slater determinant for α -spin atoms, namely, $D_\alpha = \det(e^{-i\mathbf{k}_i \cdot \mathbf{q}_i})$, the one-particle orbitals are plane waves with the $N/2$ smallest wave vectors of the form $(2\pi n/L_x, 2\pi m/L_y)$ and the 2D coordinates

$$\mathbf{q}_j = \mathbf{s}_j + \sum_{l \neq j} \eta(s_{jl})(\mathbf{s}_j - \mathbf{s}_l), \quad (3)$$

with $\mathbf{s}_j = (x_j, y_j)$, include backflow correlations [33] in the nodal structure of Ψ . Based on a comparison between fixed-node and nominally exact transient estimate (TE) results [15] for strictly 2D ${}^3\text{He}$, backflow wave functions are expected to be very accurate, at least at low density.

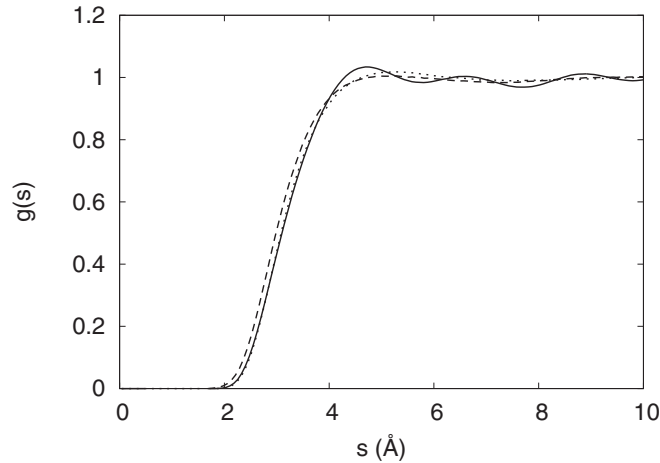


FIG. 2. Pair correlation function $g(s)$ at $\rho = 0.020 \text{ \AA}^{-2}$ for ^3He adsorbed on G (solid line) and G4He (dashed line), and for strictly 2D ^3He (dotted line). The statistical error is smaller than the thickness of the lines.

All the radial functions u , ξ , η , f , and g are parametrized as linear combinations of powers of their argument. The coefficients, a couple of negative exponents, and the shift d , for a total of about 30 variational parameters, are optimized using correlated sampling [34]. The FNDMC energies utilized in the results presented in the Sec. III include corrections for all sizable sources of bias, including an estimate of the fixed-node error [15,35], as explained in detail in Sec. IV.

III. RESULTS

The structural properties of ^3He adsorbed either on G or on G4He suggest a close similarity between the adsorbate and the strictly 2D system. The vertically integrated pair correlation function $g(s)$, where $s = \sqrt{x^2 + y^2}$, is shown in Fig. 2. For G, apart from the oscillations induced by the surface corrugation, $g(s)$ is hardly distinguishable from the 2D case. In particular, the steep rise starting at $s \sim 2 \text{ \AA}$, which defines the excluded area around each particle induced by the short-range He-He repulsion, is nearly identical for G and 2D.

This is consistent with the quasi-2D character of the film. The normalized density profile $\bar{\rho}(z) = \rho(z) / \int dz \rho(z)$, with $\rho(z) = \int dx dy \rho(x, y, z)$, is shown in Fig. 3.

On a substrate, two Helium atoms can approach the same (x, y) coordinates if their distance along z is larger than the excluded volume radius of about 2 \AA . This effectively results in a softening of the short-range repulsion with respect to the bare interparticle potential. However, as shown in Fig. 3, for G the full extent of the density profile barely reaches 2 \AA , thus leaving little room for delocalization to soften significantly the short-range repulsive part of the two-body He-He potential, in turn reducing the size of the correlation hole in $g(s)$.

For G4He, apart from the obvious shift of the peak position to the second adlayer (the first one being occupied by the ^4He solid), the density profile is almost twice as broad as for G, on account of the shallower He-substrate potential shown in the inset of Fig. 3. Nonetheless, G4He is still a relatively strong substrate, in fact slightly stronger than Mg [16] resulting in a

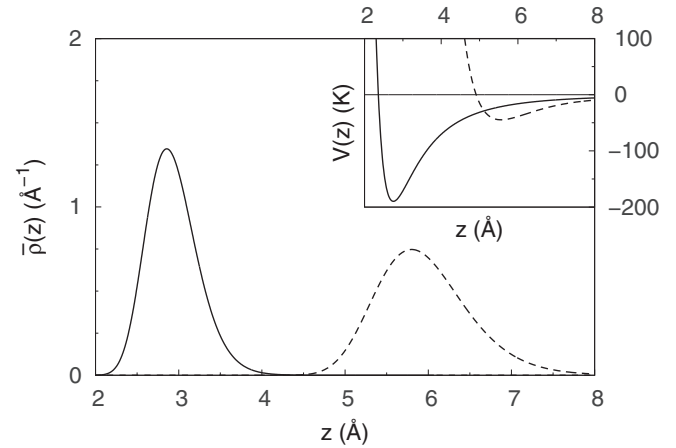


FIG. 3. Normalized density profile $\bar{\rho}(z)$ for ^3He adsorbed on G (solid line) and G4He (dashed line). The data refer to an areal density $\rho = 0.020 \text{ \AA}^{-2}$, but $\bar{\rho}(z)$ is nearly independent of ρ . The statistical error is smaller than the thickness of the lines. The inset shows the ^3He -substrate potential for G (lateral average of the anisotropic potential, solid line) and G4He (dashed line).

narrower $\bar{\rho}(z)$, a wider correlation hole in $g(s)$, and a deeper He-substrate potential, albeit not by a large amount.

In Ref. [16], a series of substrates were studied, the strongest being Mg. A local minimum was found in the EOS of ^3He adsorbed on weak alkali metal substrates, but not on Mg, so that none is expected on the even stronger G4He or G. This is indeed the case, as shown in the inset of Fig. 4. However, in a computer simulation of a system of finite size, the occurrence of a gas-liquid phase transition in a given range of density is also signalled by a *negative* value of $d\mu/d\rho$, where $\mu(\rho) = E(\rho) + \rho (dE(\rho)/d\rho)$ is the chemical potential. This is a weaker condition than the presence of a local minimum of $E(\rho)$.

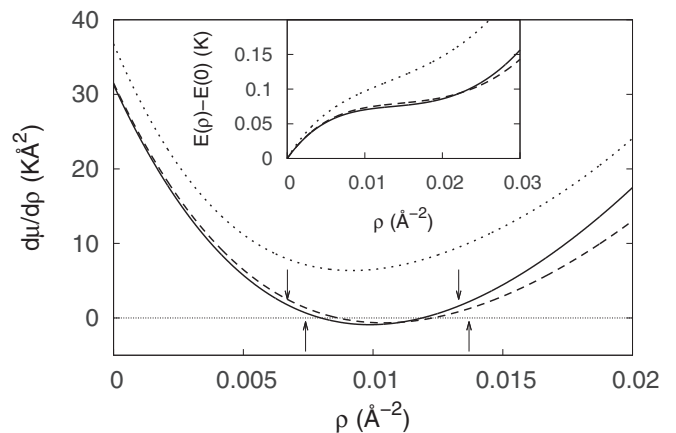


FIG. 4. Derivative of the chemical potential with respect to the density for ^3He adsorbed on G (solid line) and G4He (dashed line), and for strictly 2D ^3He (dotted line). Negative values signal instability to phase separation into a gas and a liquid phase for G and G4He, but not for 2D. Downward (upward) arrows indicate the boundaries of the coexistence region for G (G4He). The inset shows the EOS (energy per particle vs density).

TABLE I. Location ρ_{\min} and value μ'_{\min} of the minimum of the derivative of the chemical potential with respect to the density, liquefaction density ρ_L and vaporization density ρ_V of ^3He adsorbed on G and G4He. Statistical errors on the last digit(s) are given in parenthesis.

	ρ_{\min} (\AA^{-2})	μ'_{\min} ($\text{K}\text{\AA}^2$)	ρ_L (\AA^{-2})	ρ_V (\AA^{-2})
G	0.0099(3)	-0.89(25)	0.0067(6)	0.0133(7)
G4He	0.0104(1)	-0.65(11)	0.0074(2)	0.0137(4)

From a polynomial fit to the FNDMC energies calculated at several densities with statistical errors of 1.5 mK or less, we obtain the quantity $d\mu/d\rho$, shown in Fig. 4. It is clearly seen to change sign for both G and G4He in a small density interval around 0.01\AA^{-2} .

Having determined that a phase transition occurs on both G and G4He substrates (for the models considered), we locate the coexistence region by searching each EOS for two points on either side of the interval of negative $d\mu/d\rho$ with the same pressure and chemical potential. The results are listed in Table I.

Note that the coexistence regions are wider than the intervals of negative compressibility. In the intervening left and right density windows, the gas and liquid phases, respectively, are *metastable*.

While the minimum of $d\mu/d\rho$ for the 2D model has a clear bearing on the location of the coexistence regions for both G and G4He, the unexpectedly close similarity of the ^3He EOS on the two substrates should be regarded as largely fortuitous. Indeed, delocalization effects are different for G and negligible for G4He (see Sec. IV), happens to compensate nearly perfectly for that difference.

We conclude this section by mentioning, in relation to the tentative phase diagrams discussed in Ref. [18], that the ground-state energy per ^3He atom in the $\sqrt{3} \times \sqrt{3}$ solid phase commensurate with G is found in this calculation to be $E(\rho) - E(0) = 0.62(1) \text{ K}$, much higher than in the gas or liquid phases at coexistence.

IV. DETAILS OF THE CALCULATION

In this section, we discuss the sources of bias mentioned in Sec. II and the calculation of the interaction potential between a ^3He atom and the G4He substrate employed in Sec. III.

A. Sources of bias

1. Finite size effects

All the results presented in Sec. III are based on FNDMC simulations of systems of $N = 18$ ^3He atoms [36]. For the 2D system, the finite size error has been estimated from simulations of larger systems. An example is shown in Fig. 5(left) for $\rho = 0.09 \text{\AA}^{-2}$. The filled symbols indicate the FNDMC energies obtained as a function of N , with a tail correction calculated assuming $g(r) = 1$ for r larger than half the side of the simulation cell. The scatter of the data is

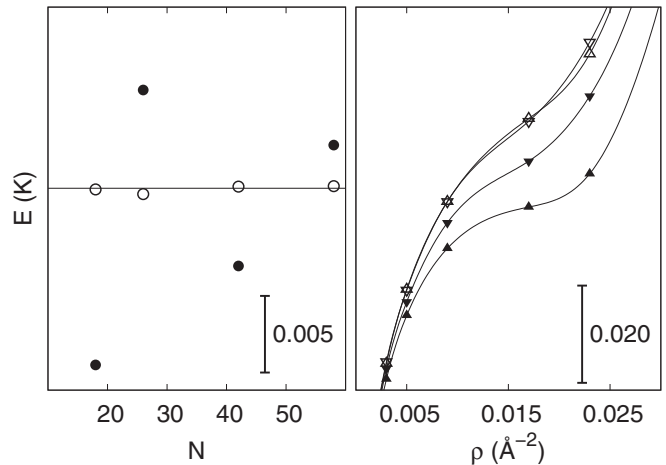


FIG. 5. (Left) FNDMC energy per particle for 2D ^3He at $\rho = 0.09 \text{\AA}^{-2}$ as a function of the number of particles: raw data (filled symbols) and values including the finite size correction of Eq. (4) (empty symbols). The line is a constant fit to the size-corrected data. (Right) FNDMC energy per particle for ^3He on G4He calculated with $N = 18$ (upward triangles) or $N = 42$ (downward triangles) as a function of density: raw data (filled symbols) and values including the finite size correction taken from the strictly 2D system (empty symbols). The lines are spline interpolations. In both panels, the statistical errors are smaller than the symbol size.

strongly reduced by applying the correction [37]

$$E(\infty) - E(N) = \alpha[T_0(\infty) - T_0(N)], \quad (4)$$

where $T_0(N)$ is the kinetic energy of a non-interacting system of N particles and α is a fit parameter [38]; this correction brings the data onto the empty symbols, which lie on a smooth curve (in fact a constant to good accuracy), which is our estimate of the energy in the thermodynamic limit. Figure 5(right) shows that the 2D size correction applied to the adsorbate on G4He (the less close to the 2D limit) gives essentially indistinguishable results for $N = 18$ and 42 . We thus conclude that the size correction of Eq. (4) with the value of α determined for the 2D case can be safely used for the adsorbates as well. No significant finite size effects were detected on the structural properties at the densities studied in the present work.

2. Time step error

For both substrates, we performed simulations with several values of the time step τ spanning an order of magnitude. We determined that the EOS $E(\rho) - E(0)$ is not affected by the time step error, within an accuracy of $\lesssim 1 \text{ mK}$, using $\tau = 5 \times 10^{-4} \text{ K}^{-1}$ for G4He and $\tau = 10^{-4} \text{ K}^{-1}$ for G. In particular, this rather conservative choice for G is due to the apparent $\tau^{1/2}$ dependence of the energy [39], shown in Fig. 6. For G4He and 2D a much weaker, linear time step dependence is observed.

3. Population control bias

This has been shown to be a potentially serious, often overlooked problem in DMC simulations [40–42]. For the low densities and small systems considered here, however, the error due to the finite number of walkers is not a concern. We

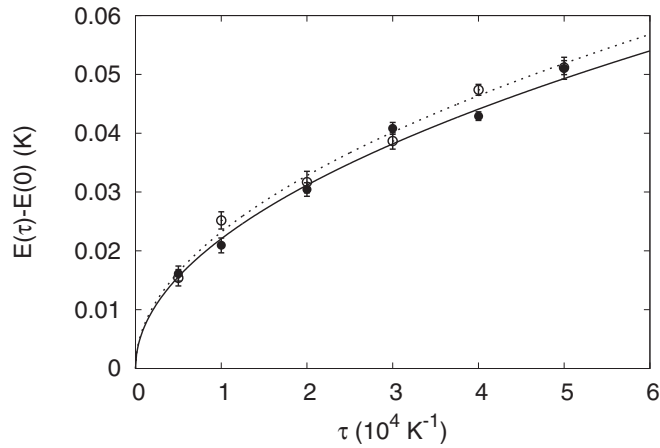


FIG. 6. Dependence of the energy E on the time step τ for ^3He on G. The filled (empty) circles with error bars are FNDMC data, and the solid (dotted) line is a fit in $\tau^{1/2}$, for $\rho = 0.005(0.020) \text{ \AA}^{-2}$.

used 6400 walkers, after verifying that this is far more than enough to eliminate this source of bias within the accuracy of the present calculations.

4. Fixed-node approximation

The FN error can be estimated from published TE results for the 2D case. From Ref. [15], a quadratic dependence on the density can be inferred, and Ref. [35] reports a FN error of $\sim 0.046 \text{ K}$ at $\bar{\rho} = 0.060 \text{ \AA}^{-2}$ using a trial function of quality comparable to those used here. We thus add a correction $-0.046(\rho/\bar{\rho})^2 \text{ K}$ to our FNDMC energies, for both the 2D and the adsorbate systems.

5. Mixed estimators

For quantities other than the total energy, the “mixed” estimators directly obtained [32] in DMC have a bias linear in the error of the trial function. The structural properties presented in this work are “extrapolated” estimators [32], whose bias is quadratic in the error of the trial function. A small difference between extrapolated and mixed estimators is often considered as a qualitative indication of small residual bias. With the trial functions used in this work, this difference is very small for the pair distribution function and barely discernible on the density profile.

B. The He-G4He potential

In a series of preliminary calculations we modeled the G4He substrate with “active” (i.e., explicitly simulated) ^4He atoms at a density $\rho_{4\text{He}} = 0.114 \text{ \AA}^{-2}$, close to the coverage where promotion to the second layer begins [2,29]. In the Jastrow factor of the trial function, namely Eq. (2), a Nosanow term [43] was added to tie the (x,y) coordinates of the ^4He atoms to the sites of a triangular lattice, and different factors $f_3(z)$ and $f_4(z)$ were used in Eq. (2) to describe localization in z for ^3He and ^4He , as well as different pair pseudopotentials u_{33} , u_{34} , and u_{44} . The corrugation of the graphite surface was not expected to have any significant effect on the ^3He atoms confined to the second monolayer

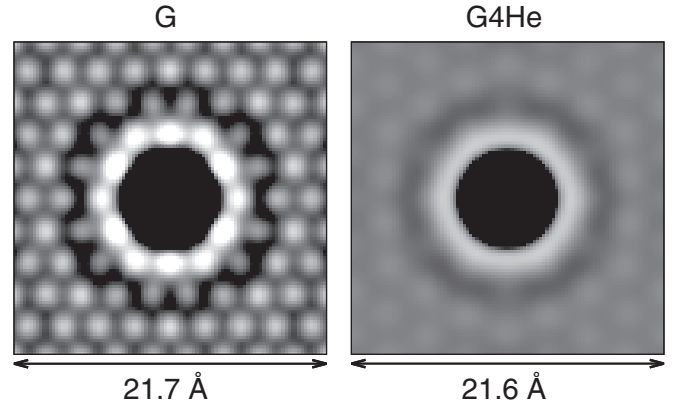


FIG. 7. Pair distribution function $g(x,y)$ for ^3He adsorbed on G at $\rho = 0.038 \text{ \AA}^{-2}$ and on G4He at $\rho = 0.038 \text{ \AA}^{-2}$. The grey-scale range, restricted to 0.94–1.19, emphasizes the long-range oscillations (the highest peaks for G reach 1.28).

by the intervening incommensurate ^4He crystal. Therefore the He-graphite interaction was described by the laterally averaged CC potential.

In the DMC simulation of a multicomponent system, the energy of a single component, such as the ^3He EOS of specific interest here, is obtained as a biased mixed estimator. Thus its projected value is influenced by all the terms in the trial function – unlike the total energy which only depends on the nodal structure. As a result, statistical fluctuations in the optimal variational parameters induce enough scattering in the density dependence of the ^3He energy to prevent us from extracting the compressibility by numerical differentiation of the EOS. Thus even neglecting the issue of the bias in the mixed (or extrapolated) estimator of the ^3He energy, the use of this “full” model turns out to be impractical. This prompts for a replacement of the ^4He layer by a rigid effective potential. To this purpose, we retain useful information on structural properties from the full model, such as the ^3He density profile of Fig. 3 and the pair distribution function of Fig. 7. In particular the density profile shows that ^3He floats atop the ^4He solid, with minimal excursions of atoms of either species in the monolayer occupied by the other, suggesting that a rigid potential is a sensible choice.

Making the further assumption of a smooth G4He substrate, we solve for the potential $U(z)$ the one-dimensional Schrödinger equation of a single ^3He atom with a known density profile,

$$U(z) = \frac{\hbar^2}{2m} \psi^{-1}(z) \frac{\partial^2 \psi(z)}{\partial z^2} + C, \quad (5)$$

where $\psi(z)$ is the square root of $\rho(z)$ calculated with the full model and C is a constant. The result for G4He is shown in the inset of Fig. 3. We assess the accuracy of this procedure on the G substrate, where the anisotropic CC potential and its smooth, laterally averaged version are both available [25]. The EOS calculated with the potential of Eq. (5) (with the density profile of a ^3He atom on the corrugated G substrate) is nearly identical to that calculated with the smooth CC potential, as shown in Fig. 8 by the dashed and the thin solid lines, respectively.

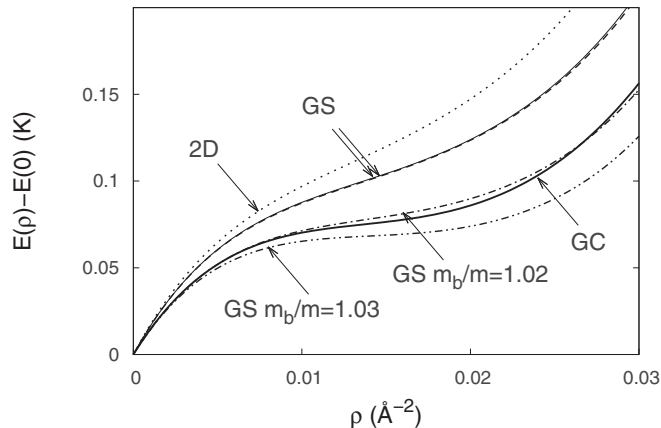


FIG. 8. EOS for ${}^3\text{He}$ adsorbed on G with various He-substrate potentials and/or effective band masses. GC (thick solid line) refers to the corrugated G substrate discussed in Sec. III. GS denotes smooth-substrate models, with either the potential of Eq. (5) (dashed line), or the laterally averaged version of the CC potential (thin solid, dash-dotted, and dash-double-dotted lines). The value m_b of the effective band mass, whenever different from the bare mass m , is as indicated. The EOS for 2D ${}^3\text{He}$ (dotted line) is also reported for reference.

Of course a smooth substrate model constructed in this way misses the corrugation effects. For the EOS of ${}^3\text{He}$ on G they are significant, as seen in Fig. 8 by comparing the results corresponding to smooth (GS) and corrugated (GC) substrates. They can be included to good accuracy into the smooth model by replacing the bare mass m of the adsorbate with an effective band mass m_b : Fig. 8 shows that the best agreement with the GC substrate is obtained using $m_b/m = 1.02$, somewhat smaller than the value $m_b/m = 1.03$ given in Ref. [25]. Incidentally, this analysis shows that the difference between the 2D system and the adsorbate on G is due more to the corrugation of the substrate than to the delocalization of the adsorbate along z .

In order to assign an effective band mass value for the G4He substrate in the lack of a reliable EOS for the full model, we compare the two-dimensional pair distribution functions $g(x, y)$ of ${}^3\text{He}$ on G and G4He in Fig. 7, whose long-range behavior is representative of the density modulation of the adsorbate induced by the corrugation of the substrate. This modulation is stronger on G than on G4He by about a factor ten, and assuming a similar ratio between the two substrates for other corrugation effects as well, we expect that for G4He the value of m_b be larger than m by only a few parts in a thousand, inducing a difference between the EOS of the smooth and the full model ten times smaller than the difference between GS and GC in Fig. 8. We consider this effect negligible and we treat G4He as a smooth substrate using the bare mass for the ${}^3\text{He}$ atoms.

V. DISCUSSION

The key result of this work, namely the change of sign of $d\mu/d\rho$ shown in Fig. 4, requires a sufficiently accurate calculation in order to be established with reasonable confidence. Although we believe that all sources of bias from the methodology adopted here are well under control (see Sec. IV),

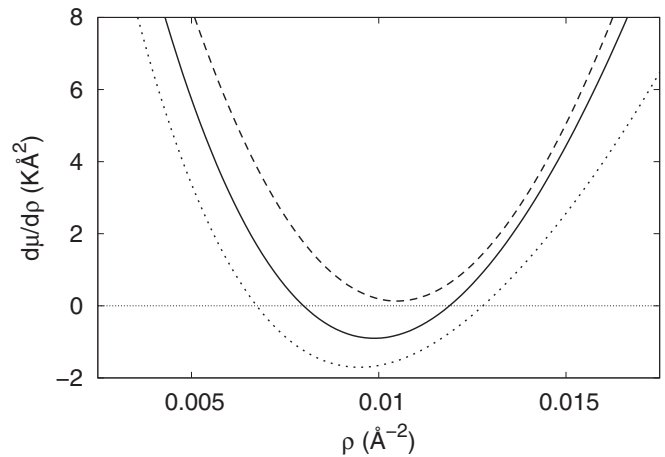


FIG. 9. Derivative of the chemical potential with respect to the density for ${}^3\text{He}$ adsorbed on G, for three different model Hamiltonians. The first (solid line) is the model of Sec. II (same as for the solid line in Fig. 4). The second (dashed line) has the He-He SAPT2 plus Axilrod-Teller potential replaced by the HFDHE2 Aziz potential. The third (dotted line) has the CC anisotropic He-G potential replaced by the smooth potential of Ref. [47] and the bare mass of the He atoms replaced by an effective band mass $m_b = 1.02m$.

we need to stress that $d\mu/d\rho$ which results from differentiating twice a fit to FNDMC energies calculated with statistical errors of the order of a millidegree of Kelvin, goes below zero by a few standard deviations. We hardly feel comfortable with the assumption that the employed model (see Sec. II), albeit of state-of-the-art level, guarantees an accuracy on the energy of the order of 1 mK throughout the relevant density range.

In order to substantiate this caution, we show in Fig. 9 that different estimates of the model Hamiltonian lead to significant differences in the result. This is the case even for the He-He interaction, arguably the most favorable case for a force-field potential. Indeed, using the HFDHE2 Aziz potential [44] instead of the SAPT2 potential supplemented with the Axilrod-Teller-Muto three-body term, the density range of negative $d\mu/d\rho$, if any, is within the statistical noise [45]. The HFDHE2 is a phenomenological pair potential which yields a fairly good equation of state [46] for bulk ${}^4\text{He}$ in 3D. On the other hand, the SAPT2 potential comes from a very accurate quantum chemistry calculation of the He dimer; in conjunction with the dominant three-body term, it is expected to afford greater accuracy than the HFDHE2, especially at low density [24].

It is important to note that the level of accuracy of either the HFDHE2 or the SAPT2 (or other modern He-He potentials) is *far* greater than that of *any* known He-graphite potential. In order to obtain a semiquantitative assessment of the amount of variation that the use of a different microscopic model for the He-graphite interaction could entail, we performed here a few calculations replacing the CC potential with the smooth He-graphite interaction of Ref. [47], with an effective ${}^3\text{He}$ band mass $m_b = 1.02m$ (see Sec. IV); to our relief, the minimum value of $d\mu/d\rho$ changes “only” by ~ 100 percent—this time in the direction of greater width of the region of negative $d\mu/d\rho$ (see Fig. 9). It should be mentioned in fairness that such a relatively limited effect arising from the replacement of the He-graphite interaction may be to some

extent accidental; in general, it is clear that a large uncertainty on our results stems from the He-graphite interaction. Indeed, there are objective limitations to the accuracy that one can achieve in describing this system by means of static potentials. In particular, the interaction between two He atoms is itself subjected to screening effects from the graphite substrate [48]. The estimated effect, larger than the differences between different versions of the He-He pair potentials [21,44], can have an influence on the delicate balance between competing phases [49,50]; in our case, it would tend to shrink or suppress the gas-liquid coexistence region (at least for the G substrate, where the ^3He adatoms are closer to the Carbon atoms). A further source of uncertainty is the motion of the Carbon atoms [51], not considered in our model Hamiltonian. Nonetheless, it seems a safe conclusion that the phase diagram of ^3He on G or G4H4 is to say the least on the edge of featuring a gas-liquid coexistence region around $\rho = 0.01 \text{ \AA}^{-2}$.

VI. CONCLUSIONS

We have performed state-of-the-art computer simulations, based on the most realistic model of the system of interest, in order to address the question of the existence of a gas-liquid phase transition of a ^3He monolayer adsorbed on a graphite substrate, either bare or preplated with ^4He . Our results, while not providing direct theoretical validation to the contended experimental observation of such a phase, reported in Ref. [20], nonetheless generally support its existence, in a region of coverage close to the experimentally relevant one.

We have attempted to offer as extensive as possible a discussion of the limitations of this calculation; as mentioned above, the most serious source of uncertainty is the microscopic model utilized.

We note that the generally unexpected phase transition characterized in Table I describes the liquefaction of a finite-pressure gas on an infinite, defect-free substrate. The specific heat should depend linearly on the density in the coexistence region, varying from the gas value at liquefaction to the liquid value at vaporization. While this is not exactly the picture of puddles on otherwise empty surfaces proposed in Ref. [20], undeniable similarities exist, most notably the density range where the effect takes place. Consideration of inhomogeneities and/or defects of the substrate in the theoretical model may bring numerical and experimental evidences in closer agreement.

It is worth mentioning that the variational Monte Carlo (VMC) calculation of Ref. [18], making use of the He-graphite potential of Ref. [47], reported evidence for a self-bound liquid. Without questioning the quality of the work of Ref. [18], or of the richness of the phase diagram of ^3He adsorbed on graphite posited therein, certainly worthy of further investigation, the existence of a self-bound liquid can be dismissed on technical grounds. For, the energy at zero density is an exact result, while at finite density the FNDMC energy is by construction lower than the VMC energy (using the same model Hamiltonian and trial function); since we find that the FNDMC EOS $E(\rho) - E(0)$ is a non-negative function, so must be the VMC EOS.

ACKNOWLEDGMENTS

This work was supported in part by the Italian MIUR through PRIN 2011 and by the Natural Science and Engineering Research Council of Canada. We acknowledge the CINECA and the Regione Lombardia award UltraQMC, under the LISA initiative, for the availability of high-performance computing resources and support. One of us (MB) gratefully acknowledges the hospitality of the International School for Advanced Studies in Trieste (Italy).

-
- [1] K.-D. Morhard, J. Bossy, and H. Godfrin, *Phys. Rev. B* **51**, 446 (1995).
 - [2] C. P. Lusher, B. P. Cowan, and J. Saunders, *Phys. Rev. Lett.* **67**, 2497 (1991).
 - [3] D. S. Greywall, *Phys. Rev. B* **41**, 1842 (1990).
 - [4] M. Boninsegni, M. W. Cole, and F. Toigo, *Phys. Rev. Lett.* **83**, 2002 (1999).
 - [5] D. J. Bishop and J. D. Reppy, *Phys. Rev. Lett.* **40**, 1727 (1978).
 - [6] G. Agnolet, D. F. McQueeney, and J. D. Reppy, *Phys. Rev. B* **39**, 8934 (1989).
 - [7] D. Tulimieri, N. Mulders, and M. H. W. Chan, *J. Low Temp. Phys.* **110**, 609 (1998).
 - [8] D. R. Luhman and R. B. Hallock, *Phys. Rev. Lett.* **93**, 086106 (2004).
 - [9] J. M. Kosterlitz and D. J. Thouless, *Prog. Low Temp. Phys.* **7**, 371 (1978).
 - [10] P. A. Whitlock, G. V. Chester, and M. H. Kalos, *Phys. Rev. B* **38**, 2418 (1988).
 - [11] A. Novaco and C. Campbell, *Phys. Rev. B* **11**, 2525 (1975).
 - [12] M. Miller and L. H. Nosanow, *J. Low Temp. Phys.* **32**, 145 (1978).
 - [13] C.-I. Um, J.-R. Kahng, Y.-S. Kim, T. F. George, and L. N. Pandey, *J. Low Temp. Phys.* **107**, 283 (1997).
 - [14] V. Grau, J. Boronat, and J. Casulleras, *Phys. Rev. Lett.* **89**, 045301 (2002).
 - [15] M. Nava, A. Motta, D. E. Galli, E. Vitali, and S. Moroni, *Phys. Rev. B* **85**, 184401 (2012).
 - [16] M. Ruggeri, S. Moroni, and M. Boninsegni, *Phys. Rev. Lett.* **111**, 045303 (2013).
 - [17] F. F. Abraham and J. Q. Broughton, *Phys. Rev. Lett.* **59**, 64 (1987).
 - [18] B. Brami, F. Joly, and C. Lhuillier, *J. Low Temp. Phys.* **94**, 63 (1994).
 - [19] H. Godfrin and H.-J. Lauter, *Prog. Low Temp. Phys.* **14**, 213 (1995).
 - [20] D. Sato, K. Naruse, T. Matsui, and H. Fukuyama, *Phys. Rev. Lett.* **109**, 235306 (2012).

- [21] T. Korona, H. L. Williams, R. Bukowski, B. Jeziorski, and K. Szalewicz, *J. Chem. Phys.* **106**, 5109 (1997).
- [22] R. D. Murphy and J. A. Barker, *Phys. Rev. A* **3**, 1037 (1971).
- [23] The energy contribution due to the three-body potential is computed perturbatively; see, for instance, P. A. Whitlock, D. M. Ceperley, G. V. Chester, and M. H. Kalos, *Phys. Rev. B* **19**, 5598 (1979).
- [24] S. Moroni, F. Pederiva, S. Fantoni, and M. Boninsegni, *Phys. Rev. Lett.* **84**, 2650 (2000).
- [25] W. E. Carlos and M. W. Cole, *Phys. Rev. B* **21**, 3713 (1980).
- [26] M. E. Pierce and E. Manousakis, *Phys. Rev. Lett.* **81**, 156 (1998).
- [27] M. Pierce and E. Manousakis, *Phys. Rev. B* **59**, 3802 (1999).
- [28] M. E. Pierce and E. Manousakis, *Phys. Rev. Lett.* **83**, 5314 (1999).
- [29] P. Corboz, M. Boninsegni, L. Pollet, and M. Troyer, *Phys. Rev. B* **78**, 245414 (2008).
- [30] P. J. Reynolds, D. M. Ceperley, B. J. Alder, and W. A. Lester, *J. Chem. Phys.* **77**, 5593 (1982).
- [31] C. J. Umrigar, M. P. Nightingale, and K. J. Runge, *J. Chem. Phys.* **99**, 2865 (1993).
- [32] M. Foulkes, L. Mitas, R. Needs, and G. Rajagopal, *Rev. Mod. Phys.* **73**, 33 (2001).
- [33] K. E. Schmidt, M. A. Lee, M. H. Kalos, and G. V. Chester, *Phys. Rev. Lett.* **47**, 807 (1981).
- [34] S. Moroni, S. Fantoni, and G. Senatore, *Phys. Rev. B* **52**, 13547 (1995).
- [35] M. Taddei, M. Ruggeri, S. Moroni, and M. Holzmann, *Phys. Rev. B* **91**, 115106 (2015).
- [36] The choice of a rather small number of ^3He atoms is motivated by the simulations of G4He substrates with active ^4He in Sec. IV B, which require very large numbers of particles at low ^3He density.
- [37] B. Tanatar and D. M. Ceperley, *Phys. Rev. B* **39**, 5005 (1989).
- [38] In order to have a smooth correction as a function of density, we use $\alpha = 0.7$, which is nearly optimal for all densities up to $\rho = 0.020$.
- [39] The time step error crucially depends on the quality of the trial function [31]. A more flexible term than the simple U_1 of Eq. (2) to represent lateral modulation for corrugated substrates would reduce the strong time step dependence observed in Fig. 6.
- [40] G. L. Warren and R. J. Hinde, *Phys. Rev. E* **73**, 056706 (2006).
- [41] N. Nemeč, *Phys. Rev. B* **81**, 035119 (2010).
- [42] M. Boninsegni and S. Moroni, *Phys. Rev. E* **86**, 056712 (2012).
- [43] L. H. Nosanow, *Phys. Rev. Lett.* **13**, 270 (1964).
- [44] R. A. Aziz, V. P. S. Nain, J. S. Carley, W. L. Taylor, and G. T. McConville, *J. Chem. Phys.* **70**, 4330 (1979).
- [45] The use of the HFDHE2 presumably explains why in Ref. [16] no gas-liquid coexistence is found for the Mg substrate, even applying with the less stringent requirement of a negative compressibility instead of the local minimum criterion followed in Ref. [16].
- [46] M. H. Kalos, M. A. Lee, P. A. Whitlock, and G. V. Chester, *Phys. Rev. B* **24**, 115 (1981).
- [47] F. Joly, C. Lhuillier, and B. Brami, *Surf. Sci.* **264**, 419 (1992).
- [48] G. Vidali and M. W. Cole, *Phys. Rev. B* **22**, 4661 (1980).
- [49] L. W. Bruch, M. W. Cole, and H.-Y. Kim, *J. Phys.: Condens. Matter* **22**, 304001 (2010).
- [50] L. Vranješ Markić, P. Stipanović, I. Bešlić, and R. E. Zillich, *Phys. Rev. B* **88**, 125416 (2013).
- [51] M. C. Gordillo, *Phys. Rev. B* **89**, 155401 (2014).